Article

Analysis of Two Quantitative Ultrasound Approaches

Ultrasonic Imaging
2018, Vol. 40(2) 84–96

DOI: 10.1177/0161734617729159
ultrasonicimaging.sagepub.com

Pauline Muleki-Seya[1], Aiguo Han[1], Michael P. Andre[2], John W. Erdman Jr.[3], and William D. O'Brien Jr.[1]

Abstract

There are two well-known ultrasonic approaches to extract sets of quantitative parameters: Lizzi–Feleppa (LF) parameters: slope, intercept, and midband; and quantitative ultrasound (QUS)–derived parameters: effective scatterer diameter (ESD) and effective acoustic concentration (EAC). In this study, the relation between the LF and QUS-derived parameters is studied theoretically and experimentally on ex vivo mouse livers. As expected from the theory, LF slope is correlated to ESD ($R^2 = 1.00$), and from experimental data, LF midband is correlated to EAC ($R^2 = 0.76$). However, LF intercept is not correlated to ESD ($R^2 = 0.25$) nor EAC ($R^2 = 0.07$). The unexpected correlation observed between LF slope and EAC ($R^2 = 0.94$) results likely from the high correlation between ESD and EAC due to the inversion process. For a liver fat percentage estimation, an important potential medical application, the parameters presenting the better correlation are EAC ($R^2 = 0.78$) and LF midband ($R^2 = 0.70$).

Keywords

quantitative ultrasound technique, QUS parameters, Lizzi–Feleppa parameters, mouse livers

Introduction

Conventional diagnostic ultrasound B-mode images are made by generating a gray-scale map using the envelope-detected radio-frequency (RF) signal backscattered from the tissues. B-mode images qualitatively display the brightness of the RF echo signal. One of the first approaches to construct quantitative ultrasonic images was an image texture analysis by fitting probability density distributions on the envelope of the RF data. These distributions could be Rayleigh, Rice, K, Homodyne K, Nakagami, or Generalized Gamma.[1,2] The parameters obtained with the image texture analysis are quantitative but system dependent. To obtain system-independent parameters, a calibration reference is needed. The frequency-dependent information of the RF data can yield estimates of attenuation coefficient (AC) and normalized backscatter power spectrum (also

[1]Bioacoustics Research Laboratory, Department of Electrical and Computer Engineering, University of Illinois at Urbana-Champaign, Urbana, IL, USA
[2]Department of Radiology, University of California at San Diego, San Diego, CA, USA
[3]Department of Food Science and Human Nutrition, University of Illinois at Urbana–Champaign, Urbana, IL, USA

Corresponding Author:
William D. O'Brien Jr., Bioacoustics Research Laboratory, Department of Electrical and Computer Engineering, University of Illinois at Urbana-Champaign, 306 N. Wright St, Urbana, IL 61801, USA.
Email: wdo@uiuc.edu

denoted backscatter coefficient [BSC]), both of which are intrinsic properties of tissue that are not dependent on the ultrasonic system or the operator.[3,4]

The early work by Kuc[5–7] and Miller[8–10] provided significant background for the later quantitative ultrasound (QUS) approaches. Two of these quantitative approaches to estimate parameters through frequency-dependent RF data were developed about the same time.[3,11] The basic methodology calls for acquiring from the region under study the echo RF signals, gate them as needed, and estimate an average power spectrum. To compensate for the system transfer function, the procedures are repeated for a known reference (planar or tissue-mimicking phantom) to generate a calibrated power spectrum. Then, normalize the average power spectrum by the calibrated power spectrum, and apply an appropriate estimated ultrasonic attenuation correction and, as needed, a diffraction correction to yield the BSC.

The first approach estimates the Lizzi–Feleppa (LF) parameters from the linear fit of the BSC and yields the slope, intercept, and midband. The second approach relies on the BSC as a function of frequency and on scatterer parameters derived from the BSC. These parameters are estimated by fitting the BSC versus frequency space with a theoretical BSC using a scattering model which yields the effective scatterer diameter (ESD) and effective acoustic concentration (EAC).

Both of these QUS methods have been applied successfully. The most common application is tissue characterization[12–20] to detect cancer,[21–29] to differentiate among cell lines,[30–33] or to characterize red blood cell aggregation.[34,35] QUS techniques are also used to detect fatty liver disease in animals[36,37] and human patients.[38,39] Kemmerer et al.[40–42] used QUS parameters to assess thermal therapy with high-intensity focused ultrasound (HIFU) in rat liver. Another application has been to monitor anticancer therapy by detecting cell death and especially apoptosis in cell pellet biophantoms,[43–45] in mouse model in vivo,[46,47] and in patients.[48]

The goal of this study is to compare the LF (slope, intercept, and midband) and QUS-derived parameters (ESD and EAC) to examine how they may be related. This relation is studied theoretically first and then experimentally using RF echo data from 40 ex vivo mouse livers. Normal and fatty mouse livers were chosen for this study, because according to previous studies,[36–39] the frequency-dependent BSC and QUS-derived parameters are expected to be correlated to the fat content.

Theoretical Correlations of QUS and LF Parameters

Scattering models are based on a 3-D spatial autocorrelation function describing the shape and distribution of scatterers in the medium.[49,50] By assuming that the scatterers have an impedance distribution and are spherical in shape, the 3-D spatial autocorrelation function leads to closed form solutions for the theoretical backscattered power spectrum. The form factor in the theoretical backscattered power spectrum describes the frequency dependence of scattering based on the size, shape, and mechanical properties of the scatterers. Using the Gaussian form factor, which represents a distribution of continuously changing impedance with the surrounding tissues, the normalized theoretical backscattered power spectrum W_{theo} is given by (see Equation (2) in Ref. 29):

$$W_{\text{theo}}(f) = \frac{185 L q^2 a_{\text{eff}}{}^6 \eta_z f^4}{1 + 2.66\left(q a_{\text{eff}} f\right)^2} \mathrm{e}^{-12.16 a_{\text{eff}}{}^2 f^2}, \tag{1}$$

where f is the frequency, L is the axial length of the range gated region (Hanning window), q is the ratio of the aperture radius to distance from the region of interest where the backscattered power spectrum is evaluated, a_{eff} is the effective scatterer radius, and η_z is the EAC ($\eta_z = \mathrm{CQ}^2$, the

product of number of scatterers per unit volume and the square of the fractional difference of acoustic impedance between the scatterers and the medium). By taking $10\log_{10}(W_{\text{theo}})$, the equation of a straight line is obtained (see Equation (14) in Ref. 29):

$$10\log\left(W_{\text{theo}}(f)\right)-10\log\left(f^4\right)\approx 10\log\left[185Lq^2{a_{\text{eff}}}^6\eta_Z\right] -4.34\left[2.66\left(qa_{\text{eff}}\right)^2+12.16a_{\text{eff}}^2\right]f^2. \tag{2}$$

The slope of this line is denoted m and depends on a_{eff}, and the intercept of this line is denoted b and depends on a_{eff} and η_Z:

$$10\log\left(W_{theo}(f)\right)-10\log\left(f^4\right)\approx m\left(a_{\text{eff}}\right)f^2+b\left(a_{\text{eff}},\eta_Z\right), \tag{3}$$

where

$$m=-\left(11.6q^2+52.8\right){a_{\text{eff}}}^2 \tag{4}$$

and

$$b=10\log\left[185Lq^2{a_{\text{eff}}}^6\eta_Z\right]. \tag{5}$$

This theoretical description does not take into account the effect of the attenuation compensation of the tissue that is implemented for the estimate of BSC. There are different techniques to estimate tissue attenuation, as the broadband insertion-loss technique[51] generally uses a planar reference for in vitro or ex vivo measurements or as the spectral difference reference phantom method[52] generally uses a reference phantom for in vivo measurements. For the planar reference method, the AC is estimated from the log difference of the reflected power spectrum from a reference reflector with and without the sample in place, and is computed as the linear slope of the frequency-dependent attenuation (in dB/cm), as developed by D'Astous and Foster[12]:

$$\alpha_s(f)=\alpha_{\text{saline}}(f)+\frac{10}{2d}\log\left(\frac{S_r(f)}{S_s(f)}\right), \tag{6}$$

where $\alpha_s(f)$ and $\alpha_{\text{saline}}(f)$ are the attenuation of the sample and the reference liquid, usually saline, respectively; $S_r(f)$ is the power spectrum of the windowed scan line from the reference measurement; $S_s(f)$ is the power spectrum of the waveform reflected from the Plexiglas plate with the sample in place; and d is the estimated sample thickness.

The spectral difference reference phantom method estimates the local attenuation using the backscattered difference in the spectral amplitude at increasing depth. The tissue within a small region of interest (ROI) is assumed to be homogeneous and isotropic. The frequency-dependent attenuation (in dB/cm) can be estimated as

$$\alpha_s(f)=\alpha_r(f)-\frac{\gamma(f)}{4\times 8.686}, \tag{7}$$

where $\alpha_r(f)$ is the attenuation of the reference phantom and $\gamma(f)$ is the slope of the straight line that fits the natural log ratio of tissue sample power spectrum as a function of depth.

To account for attenuation explicitly to estimate the LF and QUS-derived parameters, and their correlations, the attenuation compensation is applied to the normalized theoretical power spectrum W_{theo} by multiplying it by the attenuation compensation term $10^{-2z[\alpha_s(f)-\alpha_{\text{saline}}(f)]/10}$. The product of these two terms is denoted W_{att}:

$$W_{\text{att}}(z,f) = W_{\text{theo}}(z,f)10^{-2z[\alpha_s(f)-\alpha_{\text{saline}}(f)]/10}, \tag{8}$$

where z is the distance between the transducer and the gated region. Note that $\alpha_0(f)$ is expressed in dB/cm:

$$\alpha_0(f) = \alpha_s(f) - \alpha_{\text{saline}}(f). \tag{9}$$

In tissue, the attenuation is generally defined as $\alpha_0(f) = \beta_0 f^n$, where β_0 is a constant in dB/cm-MHz and n is generally close to 1 for most soft tissues. Thus, incorporating attenuation compensation, Equation (3) becomes

$$10\log\left(W_{\text{att}}(f)\right) - 10\log\left(f^4\right) \approx m\left(a_{\text{eff}}\right)f^2 + b\left(a_{\text{eff}},\eta_z\right) - 2z\beta_0 f^n, \tag{10}$$

or by denoted m_1, the slope m, with the effect of attenuation:

$$10\log\left(W_{\text{att}}(f)\right) - 10\log\left(f^4\right) \approx m_1\left(a_{\text{eff}},\beta_0 f^n\right)f^2 + b\left(a_{\text{eff}},\eta_z\right). \tag{11}$$

Note that in the case of Equation (11), there is no analytic definition for the term m_1 in the general case (especially without defining the frequency dependence of the attenuation).

Experimental QUS parameters are usually reported for a narrow frequency bandwidth due to the nature of the backscatter echo signal. Therefore, the LF and QUS-derived parameters are estimated from this narrow frequency bandwidth, and other QUS parameters, as mean BSC and mean AC, are averaged on a narrow bandwidth around the center frequency f_c. Moreover, as experimental acquisition of the backscattered echo signal data is realized over a narrow frequency bandwidth, attenuation compensation is also estimated for the center frequency. In this case, with the constant f_c, Equation (10) becomes

$$10\log\left(W_{\text{att}}(f)\right) - 10\log\left(f^4\right) \approx m\left(a_{\text{eff}}\right)f^2 + b\left(a_{\text{eff}},\eta_z\right) - 2z\beta_0 f_c^n \tag{12}$$

or

$$10\log\left(W_{\text{att}}(f)\right) - 10\log\left(f^4\right) \approx m\left(a_{\text{eff}}\right)f^2 + b_1\left(a_{\text{eff}},\eta_z,\beta_0 f_c^n\right). \tag{13}$$

The QUS method consists of fitting a straight line over $10\log(W_{\text{att}}(f)) - 10\log(f^4)$ as a linear function of f^2. The slope of this line, m, is used to estimate ESD, and the intercept b_1 is used to estimate EAC. The QUS-derived parameters ESD and EAC are defined as

$$\mathrm{ESD} = 2a_{\mathrm{eff}} = 2\sqrt{\frac{m}{11.6q^2 + 52.8}} \tag{14}$$

and

$$\mathrm{EAC} = \eta_z = 64\frac{10^{\left(b_{\mathrm{l}} + 2z\beta_0 f_c^n\right)/10}}{185Lq^2\mathrm{ESD}^6}. \tag{15}$$

The LF parameters are estimated by fitting a straight line over $10\log(W_{\mathrm{att}}(f))$ as a linear function of frequency:

$$10\log\left(W_{\mathrm{att}}\left(f\right)\right) \approx m\left(a_{\mathrm{eff}}\right)f^2 + b_{\mathrm{l}}\left(a_{\mathrm{eff}}, \eta_z, \beta_0 f_c^n\right) + 10\log\left(f^4\right). \tag{16}$$

By fitting this equation to a straight line over f, a correction factor of $2f_c$ must be used on m to estimate the slope by a linear fit:

$$\mathrm{LF}_{\mathrm{slope}} = 2f_c\left(-11.6q^2\left(\frac{\mathrm{ESD}}{2}\right)^2 - 52.8\left(\frac{\mathrm{ESD}}{2}\right)^2 + 17.4f^2\right), \tag{17}$$

$$\mathrm{LF}_{\mathrm{intercept}} = 10\log\left[185Lq^2\left(\frac{\mathrm{ESD}}{2}\right)^6 \mathrm{EAC}\right] - 2z\beta_0 f_c^n + 8.68, \tag{18}$$

$$\begin{aligned}\mathrm{LF}_{\mathrm{midband}} = {} & 2f_c\left(-11.6q^2\left(\frac{\mathrm{ESD}}{2}\right)^2 - 52.8\left(\frac{\mathrm{ESD}}{2}\right)^2 + 17.4f_c^2\right)f_c \\ & + 10log\left[185Lq^2\left(\frac{\mathrm{ESD}}{2}\right)^6 \mathrm{EAC}\right] - 2z\beta_0 f_c^n + 8.68.\end{aligned} \tag{19}$$

The simplification in the LF parameter equations is valid for frequencies expressed in GHz (because numerically, $f = 1$).

If L, q, and $\beta_0 f_c^n$ are known, then the correlation between the LF parameters—slope, intercept, and midband—and the QUS-derived parameters—ESD and EAC—can be determined (Equations (17)-(19)). LF slope is correlated to ESD. LF intercept is correlated to ESD and EAC. LF midband is correlated to ESD and EAC. It is noted that ESD is needed to estimate EAC (Equation (15)), and thus their errors are correlated. Therefore, due to the inversion process, EAC could be correlated to ESD.

Materials and Methods

Animal Protocol

The ultrasound data from this study were acquired from freshly excised livers of C57BL/6J mice. The 40 mice were fed with a control (n = 25) or a high-fat (n = 15) diet, as detailed in Ref. 36. After the RF data acquisition, the liver fat percentage was determined by a biochemical method.

Table 1. Summary of the Units of the LF and QUS-derived Parameters.

Parameter	Unit
LF slope	dB/MHz
LF intercept	dB
LF midband	dB
ESD	μm
EAC	dB/mm^3

LF = Lizzi–Feleppa; QUS = quantitative ultrasound; ESD = effective scatterer diameter; EAC = effective acoustic concentration.

QUS Methodology

RF data acquisition for mice ex vivo. Mouse livers were extracted immediately after euthanasia. Each liver was placed in a saline bath at ambient temperature for scanning. The RF data were acquired using a 40-MHz single-element transducer (NIH High-Frequency Transducer Resource Center at the University of Southern California, Los Angeles, California; diameter = 3 mm, *f*-number = 3.0, –10 dB bandwidth = [25-55] MHz, focus distance = 9.2 mm, –6 dB depth of field = 2.4 mm) excited by an UT340 Pulser-Receiver System (Utex, Science Instrument, Inc., Mississauga, Canada) connected to a personal computer (PC) analog-to-digital acquisition card with 1 GHz sampling rate. Transducer position was controlled using a Daedal Positioning System (Daedal, Inc., Harrisburg, Pennsylvania) connected to a PC running custom LabView (National Instruments, Austin, Texas) software. For each image, a Field of Interest (FOI) containing the most homogeneous part of the liver, avoiding features representing vessels on the B-mode image, was defined. The FOI contained at least 50 independent RF lines for depths included in the –6 dB depth of field of the transducer. For each liver, RF data were collected from 11 scan planes with a step size around 500 μm to estimate the BSC. The spectral estimates from the successive scans are independent.

Attenuation and BSC measurements for mice ex vivo. The attenuation for each liver was obtained using a broadband insertion-loss technique[6,51] with a 40-MHz *f*/3 focused transducer, with methodology described in Ref. 36. The attenuation was estimated from 36 independent lateral locations across the sample and averaged to obtain the mean attenuation (dB/cm) versus frequency curve over the –10 dB bandwidth 25 to 55 MHz. The BSC was estimated using the planar reference technique,[53] as described in Ref. 36: the BSC was estimated for each ROI (equivalent to 15 × 15 wavelengths at 40 MHz), and all the BSC estimates from the data of one sample were averaged together to yield the mean BSC versus frequency curve over the –10 dB bandwidth 25 to 55 MHz.

LF and QUS-derived parameters estimation. The LF and QUS-derived parameters were estimated using a fit of the BSC as a function of frequency after attenuation compensation.

The LF parameters were estimated for each mean BSC of each mouse liver. The best linear fit was estimated on 10log(BSC) versus linear frequency, and the LF parameters were extracted: slope, intercept at 0 MHz, and midband fit (amplitude in dB at the 40-MHz central frequency).

The QUS-derived parameters correspond to scatterer parameters and were extracted by fitting the BSC with a theoretical BSC using a given scattering model. As the LF method is based on a Gaussian theory, to be consistent in this study, a Gaussian form factor is used. The method to obtain the scatterer estimates (ESD and EAC) is presented in Ref. 29.

The parameter units are summarized in Table 1.

Table 2. Correlation Coefficients of the LF or QUS-derived Parameters for Ex Vivo Mouse Livers.

R^2	ESD	EAC	LF Slope	LF Intercept	LF Midband
ESD		0.98[a]	1.00[a]	0.25	0.65
EAC	0.98[a]		0.94[a]	0.07	0.76
LF slope	1.00[a]	0.94[a]		0.31	0.52
LF intercept	0.25	0.07	0.31		0.03
LF midband	0.65	0.76	0.52	0.03	

[a]Denotes that a second-order polynomial fit instead of a linear fit was used. LF = Lizzi–Feleppa; QUS = quantitative ultrasound; ESD = effective scatterer diameter; EAC = effective acoustic concentration.

The correlations among LF parameters and between ESD and EAC are presented in Figure 2, with the best linear or second-order polynomial fits. The correlation coefficients are summarized in Table 2. The LF and QUS-derived parameters are not independent; the LF slope is moderately correlated to LF midband ($R^2 = 0.55$), and ESD and EAC are strongly correlated ($R^2 = 0.98$) with a second-order polynomial fit. However, only a low correlation is observed between LF slope and LF intercept ($R^2 = 0.31$), and no correlation between LF midband and LF intercept ($R^2 = 0.03$).

Results

LF-QUS Parameters Correlations

The correlations between LF and QUS-derived parameters obtained from mouse liver data are presented in Figure 1, with the best linear or second-order polynomial fits. The correlation coefficients are summarized in Table 2. The LF slope is very well correlated to ESD ($R^2 = 1.00$) and EAC ($R^2 = 0.94$) with second-order polynomial fits. The LF midband is moderately correlated to ESD ($R^2 = 0.65$) and EAC ($R^2 = 0.76$) with linear fits. The LF intercept is not correlated to ESD ($R^2 = 0.25$) or EAC ($R^2 = 0.07$).

Correlations between LF and QUS-Derived Parameters and Fat Percentage

The correlation between fat percentage and the LF and QUS-derived parameters for ex vivo mouse livers is presented in Figure 3. The correlation coefficients for the best linear fits are summarized in Table 3. EAC presents a good correlation with fat percentage ($R^2 = 0.78$), as well as LF midband ($R^2 = 0.70$). ESD and LF slope present a moderate correlation with fat percentage ($R^2 = 0.62$ and $R^2 = 0.61$, respectively). The parameter LF intercept presents a lower correlation with fat percentage than the other parameters ($R^2 = 0.49$).

Discussion

This study focused on the theoretical and experimental correlations between LF (slope, intercept, and midband) and QUS-derived (ESD and EAC) parameters, with experimental data from ex vivo mouse livers.

Comparison of Experimental Correlations between LF and QUS Parameters with the Theory

Our theoretical expressions for LF slope and intercept (Equations (17) and (18)) were in agreement with Lizzi et al.'s[54] observations. Indeed, Lizzi et al.[54] showed that ESD was the predominant factor for the estimation of LF slope and intercept; that EAC influenced LF intercept, but not

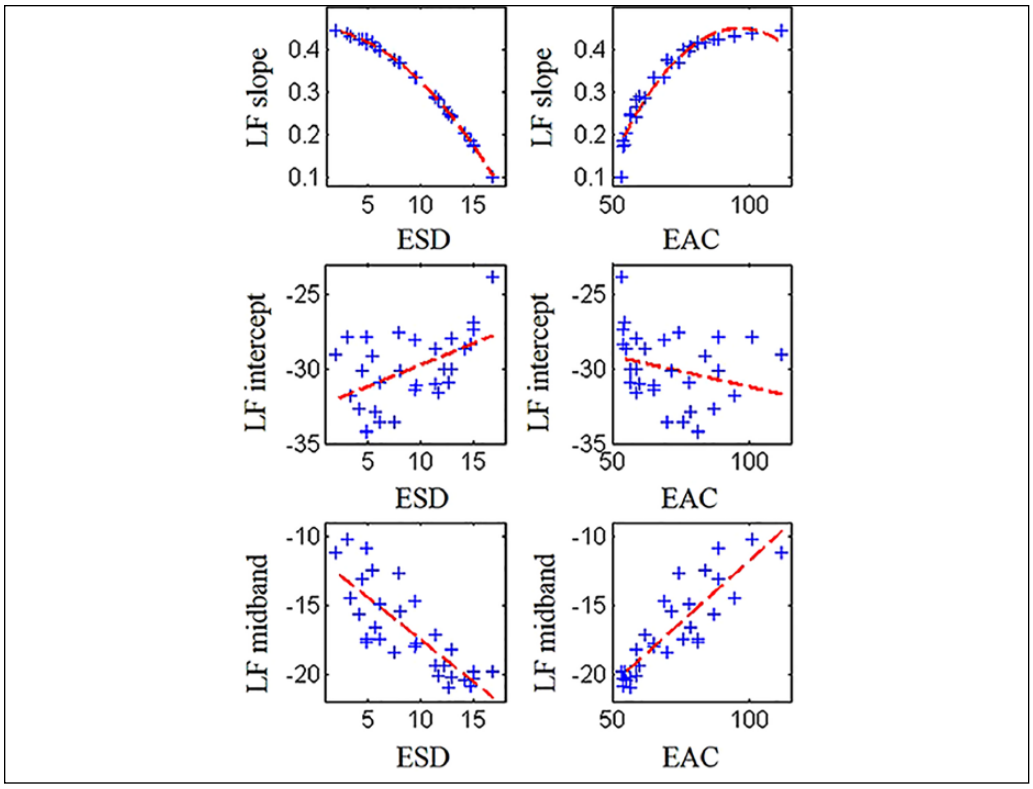

Figure 1. Correlation of LF slope, intercept, and midband with ESD and EAC. In red are plotted the best second-order polynomial or linear fits. The correlation coefficients against the null hypothesis provided p values < 0.001. LF = Lizzi–Feleppa; ESD = effective scatterer diameter; EAC = effective acoustic concentration.

LF slope; and that a large variation of EAC was necessary to change LF intercept. In our study, the LF slope depends on ESD (Equation (17)) and LF intercept depends on $(ESD / 2)^6$ and EAC (Equation (18)).

As expected from the theory (Equations (17)-(19)), the LF slope was very well correlated to ESD, and LF midband was correlated to ESD and EAC (Figure 1 and Table 2).

However, no correlation between LF intercept with ESD and EAC was apparent experimentally (Figure 1 and Table 2). An unexpected correlation was observed between LF slope and EAC (Figure 1 and Table 2). This unexpected correlation may be explained by the very good correlation between LF slope and ESD, and between ESD and EAC (Figure 2). ESD and EAC should not be correlated according to their definitions. However, as ESD is needed to extract EAC (Equation (15)), their errors are correlated, which may contribute to the correlation between ESD and EAC.

For the important fat monitoring application, LF midband and EAC may be the more appropriate of the LF-QUS-derived parameters as they present the better correlation with fat percentage for these ex vivo mouse liver data (Figure 3 and Table 3).

Effect of the Attenuation

In the general case, tissue attenuation has an effect on the BSC slope (m_1 in Equation (11)). For the LF method, an error in the attenuation compensation would lead to an error in the estimation

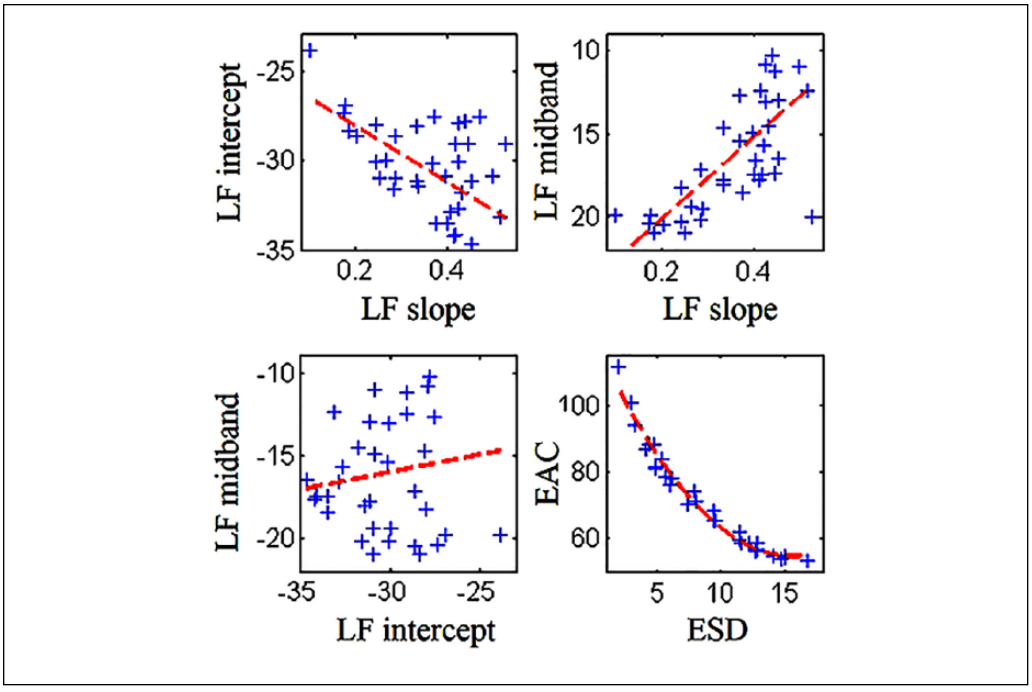

Figure 2. Correlation of LF slope, intercept, and midband among each other and correlation between ESD and EAC. In red are plotted the best second-order polynomial or linear fits. The correlation coefficients against the null hypothesis provided p values < 0.001. LF = Lizzi–Feleppa; ESD = effective scatterer diameter; EAC = effective acoustic concentration.

of the LF slope and LF midband. For the QUS method, an error in the attenuation compensation would lead to an error in the estimation of ESD and also EAC (because the value of ESD is used to estimate EAC).

For most experimental cases, the attenuation compensation is estimated using the center frequency and has an effect on the BSC intercept (b_1 in Equation (13)). For the LF method, an error in the attenuation compensation in this case would lead to an error in the estimation of the LF intercept and LF midband. For the QUS method, an error in the attenuation compensation would lead to an error in the estimation of EAC. This kind of error may explain the lack of correlation observed between LF intercept with ESD and EAC (Figure 1 and Table 2).

The use of an accurate attenuation technique may ensure a controlled experiment for this LF-QUS-derived parameters correlation study for tissue-mimicking phantoms or ex vivo tissue. When estimating the LF-QUS-derived parameters in in vivo tissue, additional errors may arise from the presence of interposed tissue between skin and liver and motion artifacts from breathing and/or vessel pulsing.

Conclusion

In this study, the relation between the LF (slope, intercept, and midband) and QUS-derived parameters (ESD and EAC) was investigated theoretically and experimentally for ex vivo mouse livers. As expected from the theory, LF slope is very well correlated to ESD, and LF

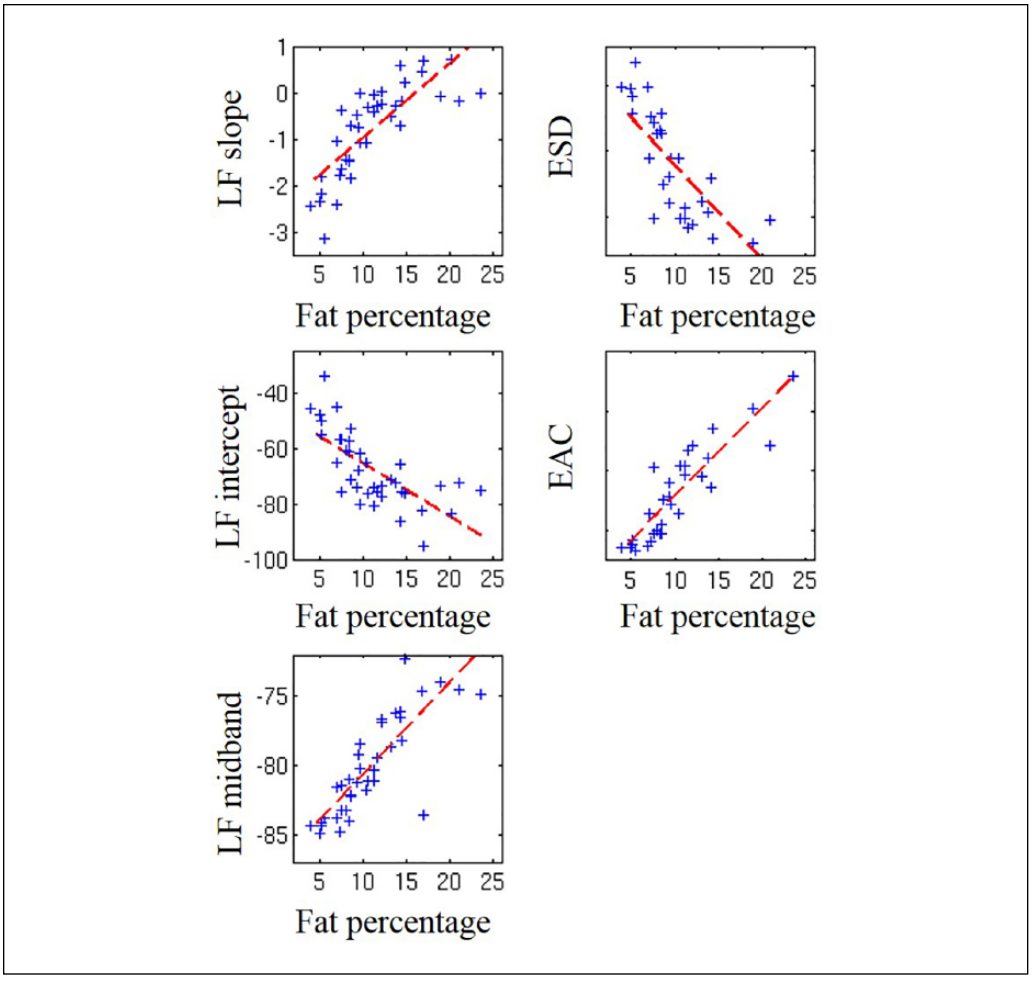

Figure 3. LF slope, intercept, and midband, and QUS ESD and EAC as a function of fat percentage. In red are plotted the best linear fits. The correlation coefficients against the null hypothesis provided p values < 0.001. LF = Lizzi–Feleppa; QUS = quantitative ultrasound; ESD = effective scatterer diameter; EAC = effective acoustic concentration.

Table 3. Correlation Coefficients of the LF and QUS-derived Parameters with Fat Percentage for Ex Vivo Mouse Livers.

R^2	ESD	EAC	LF Slope	LF Intercept	LF Midband
Fat percentage	0.62	0.78	0.61	0.49	0.70

LF = Lizzi–Feleppa; QUS = quantitative ultrasound; ESD = effective scatterer diameter; EAC = effective acoustic concentration.

midband is correlated to ESD and EAC. However, no correlation was observed between the LF intercept with ESD and EAC. An unexpected correlation was observed between LF slope and EAC, likely resulting from the very high correlation between ESD and EAC due to the inversion process.

Acknowledgments

The authors would like to thank J. R. Kelly, MS, and R. J. Miller, DVM, from the Bioacoustics Research Laboratory for the mouse liver preparation.

Declaration of Conflicting Interests

The author(s) declared no potential conflicts of interest with respect to the research, authorship, and/or publication of this article.

Funding

The author(s) disclosed receipt of the following financial support for the research, authorship, and/or publication of this article: This study was supported by National Institutes of Health Grants R37EB002641 and R01DK106419.

References

1. Oelze ML. Statistics of scatterer property estimates. In: Quantitative Ultrasound in Soft Tissues. Dordrecht: Springer; 2013. pp. 43-69.
2. Destrempes F, Cloutier G. Review of envelope statistics models for quantitative ultrasound imaging and tissue characterization. In: Quantitative Ultrasound in Soft Tissues. Dordrecht: Springer; 2013. pp. 219-74.
3. Lizzi FL, Greenebaum M, Feleppa EJ, Elbaum M, Coleman DJ. Theoretical framework for spectrum analysis in ultrasonic tissue characterization. J Acoust Soc Am. 1983;73(4):1366-73.
4. Insana MF, Hall TJ. Parametric ultrasound imaging from backscatter coefficient measurements: image formation and interpretation. Ultrason Imaging. 1990;12(4):245-67.
5. Kuc R, Schwartz M, Micsky LV. Parametric estimation of the acoustic attenuation coefficient slope for soft tissue. In: 1976 Ultrasonics Symposium, Annapolis, MD, 29 September-1 October 1976, pp. 44-47.
6. Kuc R, Schwartz M. Estimating the acoustic attenuation coefficient slope for liver from reflected ultrasound signals. IEEE Trans Son Ultrason. 1979;26(5):353-61.
7. Kuc R. Clinical application of an ultrasound attenuation coefficient estimation technique for liver pathology characterization. IEEE Trans Biomed Eng. 1980;(6):312-19.
8. O'Donnell M, Bauwens D, Mimbs JW, Miller JG. Broadband integrated backscatter: an approach to spatially localized tissue characterization in vivo. In: 1979 Ultrasonics Symposium, New Orleans, LA, 26-28 September 1979, pp. 175-78.
9. Thomas LJ, Wickline SA, Perez JE, Sobel BE, Miller JG. A real-time integrated backscatter measurement system for quantitative cardiac tissue characterization. IEEE Trans Ultrason Ferroelectr Freq Control. 1986;33(1):27-32.
10. Thomas LJ, Barzilai B, Perez JE, Sobel BE, Wickline SA, Miller JG. Quantitative real-time imaging of myocardium based on ultrasonic integrated backscatter. IEEE Trans Ultrason Ferroelectr Freq Control. 1989;36(4):466-70.
11. Madsen EL, Insana MF, Zagzebski JA. Method of data reduction for accurate determination of acoustic backscatter coefficients. J Acoust Soc Am. 1984;76(3):913-23.
12. D'Astous FT, Foster FS. Frequency dependence of ultrasound attenuation and backscatter in breast tissue. Ultrasound Med Biol. 1986;12(10):795-808.
13. Insana MF, Hall TJ, Fishback JL. Identifying acoustic scattering sources in normal renal parenchyma from the anisotropy in acoustic properties. Ultrasound Med Biol. 1991;17(6):613-26.
14. Noritomi T, Sigel B, Swami V, Justin J, Gahtan V, Chen X, et al. Carotid plaque typing by multiple-parameter ultrasonic tissue characterization. Ultrasound Med Biol. 1997;23(5):643-50.
15. Lee DJ, Sigel B, Swami VK, Justin JR, Gahtan V, O'Brien SP, et al. Determination of carotid plaque risk by ultrasonic tissue characterization. Ultrasound Med Biol. 1998;24(9):1291-99.
16. Takiuchi S, Rakugi H, Honda K, Masuyama T, Hirata N, Ito H, et al. Quantitative ultrasonic tissue characterization can identify high-risk atherosclerotic alteration in human carotid arteries. Circulation. 2000;102(7):766-70.

17. Vered Z, Barzilai B, Mohr GA, Thomas LJ, Genton R, Sobel BE, et al. Quantitative ultrasonic tissue characterization with real-time integrated backscatter imaging in normal human subjects and in patients with dilated cardiomyopathy. Circulation. 1987;76(5):1067-73.
18. Kolecki RV, Sigel B, Justin J, Feleppa EJ, Parsons RE, Kitamura H, et al. Determining the acuteness and stability of deep venous thrombosis by ultrasonic tissue characterization. J Vasc Surg. 1995;21(6): 976-84.
19. Turnbull DH, Wilson SR, Hine AL, Foster FS. Ultrasonic characterization of selected renal tissues. Ultrasound Med Biol. 1989;15(3):241-53.
20. Insana MF, Wood JG, Hall TJ, Cox GG, Harrison LA. Effects of endothelin-1 on renal microvasculature measured using quantitative ultrasound. Ultrasound Med Biol. 1995;21(9):1143-51.
21. Feleppa EJ, Lizzi FL, Coleman DJ, Yaremko MM. Diagnostic spectrum analysis in ophthalmology: a physical perspective. Ultrasound Med Biol. 1986;12(8):623-31.
22. Silverman RH, Folberg R, Rondeau MJ, Boldt HC, Lloyd HO, Chen X, et al. Spectral parameter imaging for detection of prognostically significant histologic features in uveal melanoma. Ultrasound Med Biol. 2003;29(7):951-59.
23. Feleppa EJ, Liu T, Kalisz A, Shao MC, Fleshner N, Reuter V, et al. Ultrasonic spectral-parameter imaging of the prostate. Int J Imag Syst Tech. 1997;8(1):11-25.
24. Feleppa EJ, Ennis RD, Schiff PB, Wuu CS, Kalisz A, Ketterling J, et al. Spectrum-analysis and neural networks for imaging to detect and treat prostate cancer. Ultrason Imaging. 2001;23(3):135-46.
25. Feleppa EJ, Porter CR, Ketterling J, Lee P, Dasgupta S, Urban S, et al. Recent developments in tissue-type imaging (TTI) for planning and monitoring treatment of prostate cancer. Ultrason Imaging. 2004;26(3):163-72.
26. Noritomi T, Machi J, Feleppa EJ, Yanagihara E, Shirouzu K. In vitro investigation of lymph node metastasis of colorectal cancer using ultrasonic spectral parameters. Ultrasound Med Biol. 1998;24(2): 235-43.
27. Mamou J, Coron A, Oelze ML, Saegusa-Beecroft E, Hata M, Lee P, et al. Three-dimensional high-frequency backscatter and envelope quantification of cancerous human lymph nodes. Ultrasound Med Biol. 2011;37(3):345-57.
28. Tateishi T, Machi J, Feleppa EJ, Oishi R, Jucha J, Yanagihara E, et al. In vitro diagnosis of axillary lymph node metastases in breast cancer by spectrum analysis of radio frequency echo signals. Ultrasound Med Biol. 1998;24(8):1151-59.
29. Oelze ML, Zachary JF, O'Brien WD Jr. Characterization of tissue microstructure using ultrasonic backscatter: theory and technique for optimization using a Gaussian form factor. J Acoust Soc Am. 2002;112(3):1202-11.
30. Mamou J, Oelze ML, O'Brien WD Jr, Zachary JF. Perspective on biomedical quantitative ultrasound imaging. IEEE Signal Proc Mag. 2006;23(3):112-16.
31. Mamou J, Oelze ML, O'Brien WD Jr, Zachary JF. Ultrasound characterization of three animal mammary tumors from three-dimensional acoustic tissue models. In: Proceedings of the September 2005 IEEE Ultrasonics Symposium, 2005, pp. 866-69.
32. Oelze ML, O'Brien WD Jr. Application of three scattering models to characterization of solid tumors in mice. Ultrason Imaging. 2006;28(2):83-96.
33. Oelze ML, O'Brien WD Jr, Blue JP, Zachary JF. Differentiation and characterization of rat mammary fibroadenomas and 4T1 mouse carcinomas using quantitative ultrasound imaging. IEEE Trans Med Imaging. 2004;23(6):764-71.
34. Franceschini E, Yu FTH, Destrempes F, Cloutier G. Ultrasound characterization of red blood cell aggregation with intervening attenuating tissue-mimicking phantoms. J Acoust Soc Am. 2010;127(2): 1104-15.
35. Saha RK, Franceschini E, Cloutier G. Assessment of accuracy of the structure-factor-size-estimator method in determining red blood cell aggregate size from ultrasound spectral backscatter coefficient. J Acoust Soc Am. 2011;129(4):2269-77.
36. Han A, Erdman JW Jr, Simpson DG, Andre MP, O'Brien WD Jr. Early detection of fatty liver disease in mice via quantitative ultrasound. In: 2014 IEEE International Ultrasonics Symposium, Chicago, IL, 3-6 September 2014, pp. 2363-66.

37. Ghoshal G, Lavarello RJ, Kemmerer JP, Miller RJ, Oelze ML. Ex vivo study of quantitative ultrasound parameters in fatty rabbit livers. Ultrasound Med Biol. 2012;38(12):2238-48.
38. Andre MP, Han A, Heba E, Hooker J, Loomba R, Sirlin CB, et al. Accurate diagnosis of nonalcoholic fatty liver disease in human participants via quantitative ultrasound. In: 2014 IEEE International Ultrasonics Symposium, 3-6 September 2014, pp. 2375-77.
39. Lin SC, Heba E, Wolfson T, Ang B, Gamst A, Han A, et al. Noninvasive diagnosis of nonalcoholic fatty liver disease and quantification of liver fat using a new quantitative ultrasound technique. Clin Gastroenterol Hepatol. 2015;13(7):1337-45.e6.
40. Kemmerer J, Ghoshal G, Oelze M. Quantitative ultrasound assessment of HIFU induced lesions in rodent liver. In: 2010 IEEE International Ultrasonics Symposium, San Diego, CA, 11-14 October 2010, pp. 1396-99.
41. Kemmerer JP, Oelze ML. Ultrasonic assessment of thermal therapy in rat liver. Ultrasound Med Biol. 2012;38(12):2130-37.
42. Kemmerer JP, Ghoshal G, Karunakaran C, Oelze ML. Assessment of high-intensity focused ultrasound treatment of rodent mammary tumors using ultrasound backscatter coefficients. J Acoust Soc Am. 2013;134(2):1559-68.
43. Kolios MC, Czarnota GJ, Lee M, Hunt JW, Sherar MD. Ultrasonic spectral parameter characterization of apoptosis. Ultrasound Med Biol. 2002;28(5):589-97.
44. Vlad RM, Alajez NM, Giles A, Kolios MC, Czarnota GJ. Quantitative ultrasound characterization of cancer radiotherapy effects in vitro. Int J Radiat Oncol Biol Phys. 2008;72(4):1236-43.
45. Vlad RM, Saha RK, Alajez NM, Ranieri S, Czarnota GJ, Kolios MC. An increase in cellular size variance contributes to the increase in ultrasound backscatter during cell death. Ultrasound Med Biol. 2010;36(9):1546-58.
46. Banihashemi B, Vlad R, Debeljevic B, Giles A, Kolios MC, Czarnota GJ. Ultrasound imaging of apoptosis in tumor response: novel preclinical monitoring of photodynamic therapy effects. Cancer Res. 2008, 68:8590-8596.
47. Vlad RM, Brand S, Giles A, Kolios MC, Czarnota GJ. Quantitative ultrasound characterization of responses to radiotherapy in cancer mouse models. Clin Cancer Res. 2009;15(6):2067-75.
48. Sadeghi-Naini A, Papanicolau N, Falou O, Zubovits J, Dent R, Verma S, et al. Quantitative ultrasound evaluation of tumor cell death response in locally advanced breast cancer patients receiving chemotherapy. Clin Cancer Res. 2013;19(8):2163-74.
49. Insana MF, Wagner RF, Brown DG, Hall TJ. Describing small-scale structure in random media using pulse-echo ultrasound. J Acoust Soc Am. 1990;87(1):179-92.
50. Lizzi FL, Astor M, Liu T, Deng C, Coleman DJ, Silverman RH. Ultrasonic spectrum analysis for tissue assays and therapy evaluation. Int J Imag Syst Tech. 1997;8(1):3-10.
51. Wear KA, Stiles TA, Frank GR, Madsen EL, Cheng F, Feleppa EJ, et al. Interlaboratory comparison of ultrasonic backscatter coefficient measurements from 2 to 9 MHz. J Ultrasound Med. 2005;24(9):1235-50.
52. Yao LX, Zagzebski JA, Madsen EL. Backscatter coefficient measurements using a reference phantom to extract depth-dependent instrumentation factors. Ultrason Imaging. 1990;12(1):58-70.
53. Chen X, Phillips D, Schwarz KQ, Mottley JG, Parker KJ. The measurement of backscatter coefficient from a broadband pulse-echo system: a new formulation. IEEE Trans Ultrason Ferroelectr Freq Control. 1997;44(2):515-25.
54. Lizzi FL, Ostromogilsky M, Feleppa EJ, Rorke MC, Yaremko MM. Relationship of ultrasonic spectral parameters to features of tissue microstructure. IEEE Trans Ultrason Ferroelectr Freq Control. 1987;34(3):319-29.